

# Velocity Determination in High Enthalpy Ground Testing Facilities

Stefan Löhle<sup>†</sup>, Torsten Laux<sup>‡</sup>, Monika Auweter-Kurtz<sup>†</sup>

<sup>†</sup>Institut für Raumfahrtssysteme  
 Universität Stuttgart, Pfaffenwaldring 31, D-70550 Stuttgart  
 Tel.: +49-(0)711-685-2394, Fax: +49-(0)711-685-3596  
 e-mail: loehle@irs.uni-stuttgart.de

<sup>‡</sup>Institute of Structures and Design  
 German Aerospace Center, Pfaffenwaldring 38-40, D-70569 Stuttgart  
 Tel.: +49-(0)711-6862-684, Fax: +49-(0)711-6862-227

## Abstract

The flow velocity is of significant importance in plasma wind tunnels, because the enthalpy and hence the chemical reaction processes in the boundary layer near the surface consist mainly of the high velocity. In real re-entry scenarios, the plasma is resulting from the strong bow shock in front of the vehicle which is again the result of the high velocity. In this paper, a comparison is made between the theoretically estimated velocity from basic equations for hypersonic flow conditions and experimentally gained velocities using Fabry-Perot-Interferometry. This optical diagnostic means is used in the present investigation to measure the translational temperature and velocity of nitrogen atoms. Depending on the ambient pressure, velocities between 1000 m/s and 4000 m/s have been measured. The detectability limit is the emission spectra of the flow which is influenced by the oxygen mass flow and the input power of the generator. Under the assumption of chemical equilibrium, several possible comparisons are made leading to the result that the pure nitrogen flows are considerably in non-equilibrium.

## 1 Introduction

Investigations of thermal protection systems (TPS) are currently being made by numerical calculations and plasma wind tunnel experiments [1]. The purpose of the experimental investigations is mainly to understand the chemical behaviour of the TPS that is used. At Institute for Space Systems (IRS), several plasma wind tunnel concepts are in operation and they mainly differ in their pressure and enthalpy envelopes. According to a certain re-entry trajectory, in a plasma wind tunnel, the chemical and thermal loads onto the surface of the vehicle can be simulated. Figure 1 shows

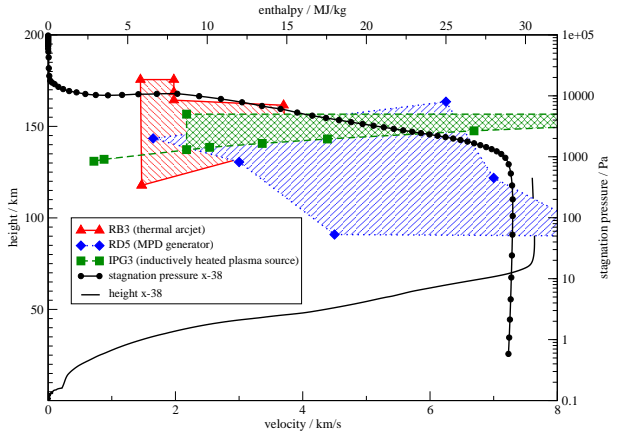


Figure 1: Simulation capabilities at IRS together with X-38 trajectory

the envelopes together with the predicted trajectory for the X-38. Additionally, the plasma generators can be driven with different gas composition which is of particular interest for the described material research.

As can be seen from Fig. 1, the enthalpy is one of the essential values for a reliable re-entry simulation in plasma wind tunnels. The on-stream conditions naturally depend on the position of a certain probe in the flow. In principle, total specific enthalpy of a streaming gas is defined by

$$h = c_p T + \frac{1}{2} v^2, \quad (1)$$

where,  $c_p$  stands for the specific heat of the investigated species,  $T$  is its temperature, and  $v$  is the velocity of the flow. The high enthalpy condition in the real re-entry scenario is due to the high velocity of the vehicle which leads to a strong bow shock in front of the blunt nose of the vehicle. This means, the high enthalpy condition originates from the second term in

Eq. 1. In plasma wind tunnels, high enthalpy conditions are generated by expansion of a heated gas through a nozzle. The reached velocities are much lower than in an original re-entry case and the first term in Eq. 1 is of importance, too. In order to investigate the high enthalpy condition, it is necessary to know both, the velocity and the temperature of the flow. Since the re-entry plasma flows as well as the experimental ones are in chemical and thermal non-equilibrium, usually the translational temperature is chosen for calculations. In the present investigation, the velocity at several supersonic plasma conditions is determined using Fabry–Perot–Interferometry (FPI). The results are compared to analytically estimated velocities using Pitot pressure measurements in plasma wind tunnels. The theoretical approach is described and an outlook is given that the measured velocities are below theoretical values which leads to a conclusion that by using the theoretical approach a more or less conservative estimation of velocity is possible.

## 2 Theory

The following paragraphs describe the theoretical approach to estimate the local velocity followed by the theoretical description of the Fabry–Perot–Interferometric setup.

### 2.1 Pitot pressure measurements

The flow velocity  $v_\infty$  of the free stream can be calculated from the speed of sound  $a_\infty$  and the Mach number  $M_\infty$ :

$$v_\infty = M_\infty \cdot a_\infty . \quad (2)$$

For the determination of  $M_\infty$  it has to be distinguished between a subsonic or supersonic flow. In the present case of a supersonic flow, the so-called Rayleigh–Pitot equation is used to calculate the Mach number depending on the stagnation pressure and the static pressure:

$$\frac{p_0}{p_\infty} = \left( \frac{\kappa + 1}{2} \cdot M_\infty^2 \right)^{\frac{\kappa}{\kappa - 1}} \cdot \left( \frac{2 \cdot \kappa}{\kappa + 1} \cdot M_\infty^2 - \frac{\kappa - 1}{\kappa + 1} \right)^{\frac{1}{1 - \kappa}} . \quad (3)$$

Here,  $\kappa$  is the isentropic exponent. The equation must be solved iteratively. The ratio of the pressure in stagnation point  $p_0$  to pressure in the flow  $p_\infty$  is approximately the ratio of the measured Pitot pressure to the chamber pressure:

$$\frac{p_0}{p_\infty} \approx \frac{p_{Pitot}}{p_{ch}} \quad (4)$$

A mean temperature between 5000 and 6000 K gives a speed of sound of 1500 m/s and an isentropic exponent

of 1.1. The temperature range is deduced from heat flux measurements, which allow the estimation of the enthalpy according to POPE's theory [2]:

$$h_\infty \approx \frac{q_{fc}}{K \sqrt{\frac{p_{Pitot}}{R_{eff}}}} . \quad (5)$$

with fully catalytic heat flux as:

$$\dot{q}_{fc} = 1.25 \cdot \dot{q}_{Cu} , \quad (6)$$

the effective nose radius:

$$R_{eff} = 2.9 \cdot R_{Probe} . \quad (7)$$

and the constant  $K=342 \text{ W}/(\text{MJ}/\text{kg} \cdot \text{Pa}^{0.5} \cdot \text{m}^{1.5})$ . Furthermore, mass spectrometer measurements are used to estimate the composition of the plasma flow. With the enthalpies and the compositions at two different pressure levels of  $p = 1013 \text{ Pa}$  and  $p = 10130 \text{ Pa}$  the mean temperature can be estimated. Putting Eq. 3 and the definition for the MACH number together (Eq. 2), the estimation of the velocity is possible. More detailed explanations are given in [3].

### 2.2 Fabry–Perot–Interferometry

In this section the theoretical approach to estimate the velocity using Fabry–Perot–Interferometry is described in detail.

The experimental principle of Fabry–Perot–Interferometry is to measure the emission of an atomic line with very high resolution. Two mirrors are installed at an adjustable distance through which the light emitted by the plasma is fed (see Fig. 6). The light enters the interferometer from one side, passes the mirror and is reflected several times between the mirrors before it exits the interferometer through the other mirror. The distance between the mirrors can be adjusted with high accuracy. In modern setups, the mirrors are moved using piezo–electric motors and ramp generators. The measured intensity is recorded using oscilloscopes. When the distance of the mirrors is  $n$  times half the wavelength of an emission line of an atom or molecule, constructive interference occurs. Then, on the oscilloscopes, one or more discrete maxima can be observed. From the evaluation of the line shape, its broadening and the shift between the observation of two emissions under known view angles, the velocity and translational temperature can be estimated. The background physics are explained in the following two paragraphs.

The thermal broadening of an emission line is

$$\Delta\lambda_T = 2\lambda_0 \sqrt{\frac{2k T_{tr} \ln(2)}{m c^2}} , \quad (8)$$

where  $k$  is BOLTZMANN's constant,  $m$  the relative atomic weight of the particle under investigation,  $c$  the

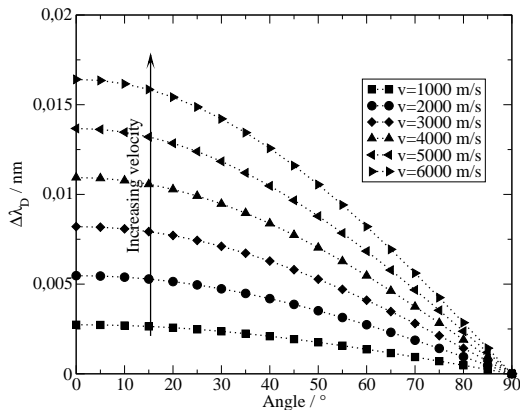


Figure 2: Expected DOPPLER–shift for assumed velocities at a nitrogen emission line of  $\lambda_0 = 821$  nm and varying view angle

speed of light,  $\lambda_0$  the centre of the emission line, and  $T_{tr}$  the translational temperature [4]. The broadening of the measured line is the addition of the so–called instrumental broadening and the thermal broadening leading to

$$\Delta\lambda_{ges}^2 = \Delta\lambda_{instr.}^2 + \Delta\lambda_T^2. \quad (9)$$

The instrumental linewidth is measured using a known emission line. A HeNe–Laser is used and its wavelength and broadening is measured using a wavemeter (ATOS–Lambdameter).

In order to measure velocities, two separate measurements are needed. This is pictured in Fig. 6. The velocity is hence estimated by applying the DOPPLER–effect. Measuring the same emission line orthogonal to the flow direction and under a certain known angle leads to two slightly shifted emission lines. The axial velocity  $v_x$  can be estimated when the commonly known equations for the DOPPLER–effect are solved resulting in

$$v_x = \frac{\Delta\lambda_D c}{\lambda_0 \cos\alpha}, \quad (10)$$

wherein  $\Delta\lambda_D$  stands for the measured shift and  $\alpha$  is the used angle. Measurements orthogonal to the flow, i.e. under  $90^\circ$  are not affected by a DOPPLER–shift. Therefore, it can be used as the reference emission line at  $\lambda_0$  [4]. The theoretically best view angle would be in flow direction which is not feasible, therefore, an angle of  $45^\circ$  is used.

The calculated shift for assumed velocities is depicted in Fig. 2 using an emission line of atomic nitrogen at  $\lambda_0 = 821$  nm.

As can be seen, the expected difference is extremely small. This is one of the major reasons, why a Fabry–Perot–Interferometer has to be used. With a conventional spectrometer, the resolution to extract these small deviations is not high enough.

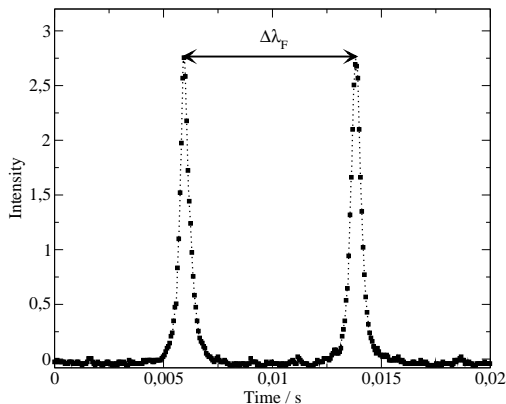


Figure 3: Measured calibration emission of a HeNe–Laser at  $\lambda = 633$  nm

In practise, the moving mirror plate generates the emission lines on an oscilloscope, i.e. intensity versus time. Hence, the needed wavelength (see Eq. 10 and 8) has to be derived. By varying the distance of the mirror plates, one or more constructive interferences of the emission line under investigation can be measured. Usually, two lines are plotted which is depicted exemplarily in Fig 3.

The distance between the mirrors can be measured using a simple calliper gauge. When the emission line is known as it is for example the case when a laser is used, the free spectral width  $\Delta\lambda_F$  is

$$\Delta\lambda_F = \frac{\lambda_0^2}{2d}. \quad (11)$$

Here,  $\lambda_0$  is the known laser wavelength and  $d$  the distance between the mirrors. This calculation is independent from the oscilloscope and its time scale, but the distance between two constructive interferences is the free spectral width, too, i.e.

$$\Delta\lambda_F = m_2 - m_1. \quad (12)$$

The two maxima  $m_1$  and  $m_2$  are read out as seconds on the oscilloscope’s time scale. From the Eqs. 11 and 13 the seen distance in seconds can be calculated to a real length, e.g. in meters. Usually, it is written as a correction factor  $K$  in the form

$$K = \frac{\Delta\lambda_F/\text{nm}}{\Delta\lambda_F/\text{s}}. \quad (13)$$

For better data analysis, the measured signal is averaged and a fit using two Gaussian curves is applied.

### 3 Experiments

The experimental setup is divided into two parts. Firstly, the description of the plasma wind tunnel facility and secondly, the hardware adapted for the FPI–measurements.

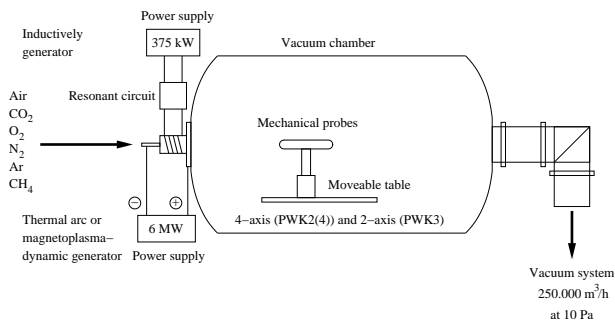


Figure 4: Schematic of the plasma wind tunnels at IRS

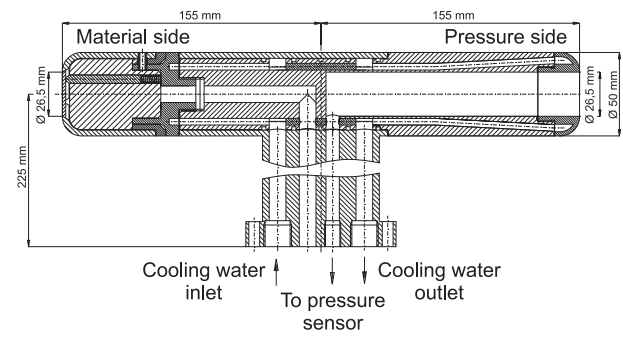


Figure 5: Double probe for material investigations and Pitot pressure measurements

Table 1: Experimental conditions

No.	$I/A$	$p_a/\text{Pa}$	$p_{tot}/\text{Pa}$	$\dot{m}_{N_2}/\text{g/s}$
1	800	60	686	5
2	500	500	2976	5
3	500	1000	4013	5,5

### 3.1 Plasma Wind Tunnels

Plasma wind tunnels are facilities for the partial recreation of re-entry conditions, mainly used to qualify thermal protection materials. In general, they consist of a vacuum tank, a pump system for low ambient pressure conditions, a plasma source to generate the high enthalpy plasma flow, a suitable power supply system, auxiliary components such as a gas and cooling water, and the measurement equipment and data processing system (see Fig. 4).

The present study has been performed in the arc heated plasma wind tunnels PWK1(4) and PWK2(4). Their water cooled vacuum chambers are 5 m in length with a diameter of 2 m. Each chamber is equipped with a 4-axis positioning system on which the various probes for plasma diagnostic or specimen support systems can be mounted. In the coaxial thermal plasma generator RB3 the test gas is heated up in the discharge chamber by an electric arc and accelerated in a nozzle. Since contact between the oxygen in the test gas and the cathode has to be avoided, the air plasma has to be simulated. Nitrogen is passed along the cathode into the plenum chamber while oxygen is injected at the downstream end of the anode near the nozzle throat [5]. In order to measure and observe the plasma as well as to optically measure surface temperatures of material samples, windows are mounted on both vacuum chambers. Both tunnels are connected to a four stage vacuum pump system that can simulate pressures down to 10 Pa [5].

Three different conditions are investigated. The generator parameters and the measured total pressure are presented in table 1.

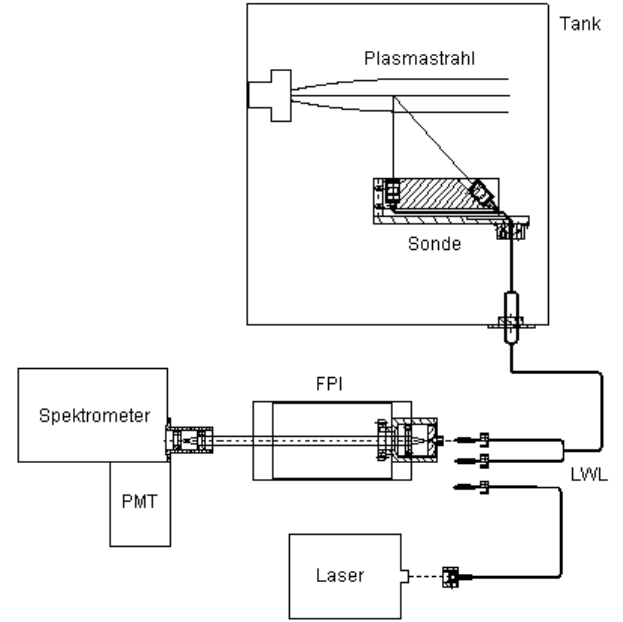


Figure 6: Schematic of the Fabry-Perot-Interferometric setup

### 3.2 Diagnostics

The Pitot pressure measurements were performed using a double probe which allows material tests as well as Pitot pressure measurements in stagnation point configuration. The probe has an outer diameter of 50 mm, while the size of the sample or the orifice for pressure measurement is 26.5 mm (see Fig. 5).

At IRS, a BURLEIGH interferometer is in operation. As described, for velocity measurements, the DOPPLER-effect is used. Therefore, the emission has to be measured orthogonal and under  $45^\circ$  to the flow direction. In order to measure the velocity in a low density flow which necessitates a low pressure environment, a fibre optical setup is used. The interferometer and the used spectrometer to separate wavelengths are outside the vacuum chamber and only a water-cooled probe is installed nearby the plasma flow. Figure 7 shows the used probe. It consists of two lens systems. Each is



Figure 7: Probe to measure the emission lines under  $90^\circ$  and  $45^\circ$



Figure 8: Picture of the data acquisition hardware

used to image the same position in the flow, 32 mm above the probe, onto the entrance of the fibre optics cable. The end of the fibre is mounted on the entrance of the FPI. Actually, the measurements are made separately by mounting the fibre for  $90^\circ$  and after recording the spectra, the fibre for  $45^\circ$  view angle is mounted (see Fig. 6).

The FPI itself uses a lens to widen the beam before it passes the mirrors. The mirrors are adjusted by three knobs to get a homogeneous interference pattern which strongly depends on the parallel adjustment of the mirrors. To separate the emission, an additional spectrometer is used for wavelength separation. The output is finally recorded using a photomultiplier tube of type HAMAMATSU R955. The oscilloscope to be used is a two channel storage oscilloscope (AGILENT), which allows averaging and can be read out by a computer for data acquisition.

As already mentioned, the thermal arc-jet generator RB3 generates a supersonic plasma flow with an under-expanded free stream. Hence, regions of ex-

pansion and shock fronts results in the free stream. The flow velocity is decreasing with several discrete velocity losses at the shock position. In the present investigation, the position of the probe has an important influence on the velocity. A comparison can be made when the FPI-measurements and the probe measurements are performed at the same position. Unfortunately, the minimum distance of the quite long FPI-probe is 240 mm from the generator's nozzle exit. Some measurements of interest (see LAUX [3]) are at  $x = 180$  mm. The decrease in velocity using the total pressure probe and the Eqs. 2 and 3 leads to the assumption that in between these 60 mm, no significant velocity change should be measured.

## 4 Results

In the following two paragraphs the results are described.

### 4.1 Nitrogen Flows

The optical measurements were performed using the atomic nitrogen emission line at  $\lambda = 821$  nm. Figure 9 shows an exemplary resulting plot of a measurement under  $90^\circ$ , i.e. orthogonal to the flow direction, and under  $45^\circ$ .

The diagram shows three different lines. For the unshifted line under  $90^\circ$ , only the Gaussian fit is depicted. The recorded data for the view angle  $45^\circ$  is shown in grey and the fit is shown with the broken line. As can be seen, the  $90^\circ$ -fit and the  $45^\circ$ -fit are shifted. This is due to the DOPPLER-effect. In fact, there can be two maxima identified for each order. This is due to the fact, that the atomic nitrogen emission line at 821 nm has two fine structure levels at  $\lambda = 821,632$  nm,  $\lambda = 821,18$  nm. These maxima

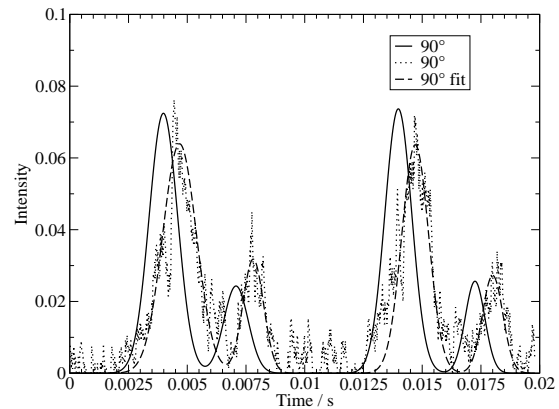


Figure 9: Fabry-Perot interferometric result for flow condition 1

Table 2: Results for the three flow conditions

No.	$v_{tot}$ / m/s	$v_{FPI}$ /m/s	$T_N$ /K
1	$5263 \pm 1403$	$3761 \pm 140$	9200
2	$3375 \pm 900$	$1875 \pm 64$	7100
3	$2702 \pm 721$	$685 \pm 477$	7400

can naturally be identified by a high resolution FPI-measurement.

From the measurement of the shift the velocity can be estimated. The broadening of the line gives the translational temperature. Table 2 shows the measured results by FPI and the estimated ones by Pitot pressure measurements.

The deviations in the FPI-measurements are calculated from the evaluation of all four maxima. Since the data fit is made using four Gaussian curves that are summed to one curve (see Fig. 9), each Gaussian curve can be moved and positioned for one maxima of the measured data. The deviations in the theoretically calculated values are due to the uncertainties of the estimation of the Mach number and the speed of sound. Additionally, FPI-measurements have about 30% of error [4]. Taking into account these deviations, the results are indeed comparable. However, there are several possible reasons for the deviation as will be explained below.

First, as already mentioned, at test condition 1 the axial position is slightly different. A simple calculation using the principle of linear momentum results in a lower velocity at a distance farther away from the generator of about 1000 m/s. So, the deviation is probably a result of the different positions.

A second possibility can be the different experimental estimation of the velocity. Indeed, since the line shift resulting from the different view angle are very small (see Fig. 2), the velocity measurement error is about 30%. But the temperature estimation is much lower sensitive with respect to best Gaussian fit. Therefore, the velocity additionally has been estimated using the temperature from the FPI-measurements. Furthermore, chemical equilibrium is assumed. Using the equations 2 and 3 the velocities are 8600 m/s, 4900 m/s, and 5000 m/s for the flow conditions 1–3, respectively. The isentropic exponent is  $\kappa = 1,1$  and the Mach number is taken from the total pressure measurements. However, these velocities are far too high. This indicates, that the measured temperature (from Tab. 2 is not useful for an equilibrium calculation.

Finally, the last approach to extend the measured data is to calculate the enthalpy from chemical equilibrium depending on temperature. Again, the Mach numbers are taken from the pressure measurements. Together with the measured heat flux data, according to MARVIN and POPE, the enthalpy can be estimated. In Fig. 10, the enthalpy is plotted versus temperature.

For the estimated enthalpies at flow conditions 1–3, the resulting temperatures are 4800 K, 4900 K, and 5300 K. These equilibrium temperatures are below the temperatures estimated by the FPI-measurements.

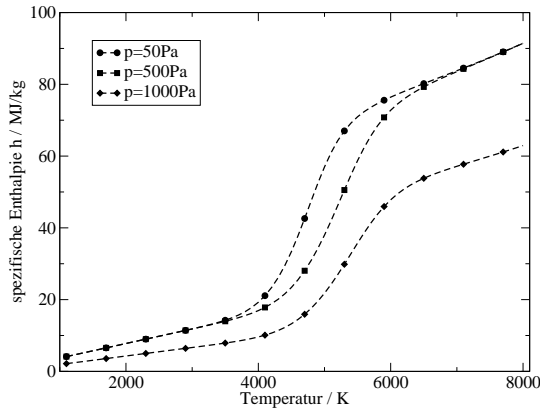


Figure 10: Calculated enthalpy assuming chemical equilibrium as a function of temperature

This leads to the assumption that the chemical non-equilibrium is of considerable influence. Probably, the nitrogen atom is highly excited leading to the by FPI measured high temperatures and hence to an underestimation of the velocity using chemical equilibrium assumptions. The measured velocities  $v_{FPI}$  and the calculated velocities  $v_{tot}$  assuming chemical equilibrium from the beginning, i.e. without using the temperature measurement, leads to velocities within the error range of the FPI-measurements.

## 4.2 Nitrogen-Oxygen Flows

For the investigation of material behaviour during a re-entry flight, one is interested in air plasma. Currently, materials using silicon carbide protection layers are favoured. These materials complain differently depending on the oxygen partial pressure and temperature [3]. At certain conditions, a so-called passive to active transition occurs ongoing with a sudden temperature increase and much higher specific material loss. At IRS, measurement techniques are in use to investigate this behaviour [1]. Recent material investigations show that the flow velocity has an influence on the transition from passive to active oxidation and reverse. The measurements of LAUX in pure nitrogen showed also that the rest of oxygen in the vacuum chamber under so-called pure nitrogen conditions can trigger these transition process. Nevertheless, the investigation of oxygen emission lines are of special interest. Unfortunately, the used fibre optics setup could not be used for oxygen measurements. As an additional investigation, the generator is driven with nitrogen and oxygen is added. The plasma state changes and the nitrogen emission line disappears at higher oxygen mass

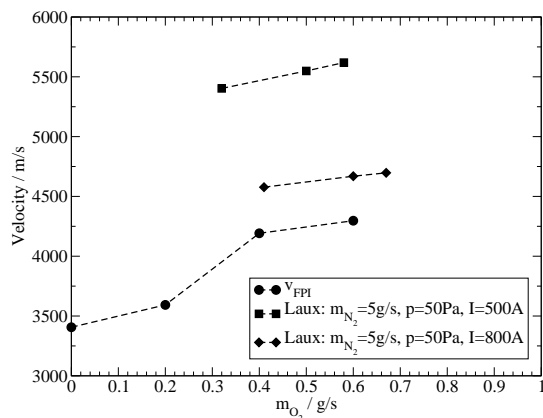


Figure 11: Velocity as a function of the oxygen mass flow; [3]

flows. A real air composition has not been reached. Figure 11 depicts the results together with investigations from LAUX.

The tendency is obvious. The velocity increases due to the higher total mass flow and the same result is seen from the equilibrium calculations. As already concluded at the three flow conditions discussed above, the measured velocities are lower than the calculated ones.

The effect, that the nitrogen emission line disappears at higher oxygen mass flows, underlines the assumption of highly excited nitrogen in flow conditions 1–3. The additional mass flow results in lower excitation of the nitrogen and hence in a lower emission.

## 5 Conclusion and Outlook

In this paper, a comparison is made between theoretically calculated flow velocities from total pressure measurements and the assumption of chemical equilibrium and Fabry–Perot–Interferometry. For the three flow conditions the measured velocity from FPI-measurements is lower than the theoretically estimated ones. The temperatures evaluated from the line broadening is in good agreement with the approach to use Pitot pressure and heat flux measurements. The measurements with varying oxygen mass flow shows the same tendency for the resulting free stream velocity as predicted by LAUX. Since the transition from passive to active oxidation is additionally influenced by the flow velocity, it is important to know the flow velocity. In combination with the material tests of LAUX further investigations can now be performed using the velocity measurements or the velocity estimation from pressure measurements knowing that this velocity  $v_{tot}$  is slightly too high.

Further improvements could be done using better fibre

optics leading to higher efficiency of the transmission and in consequence to the possibility to investigate for example atomic oxygen emission lines. In supersonic flows, it is additionally necessary to perform total pressure measurements to find out the position of the shock fronts. At these positions, where discrete changes in all flow characteristics are present, the evaluation of the deviations between the  $45^\circ$  and  $90^\circ$  is not feasible.

## Acknowledgement

The authors wish to thank all the laboratory people for their support during the test campaign and Dipl.–Ing. M.Winter for his help with the optical setup and Dipl.–Ing. H.Böhrk for the review of the paper.

## References

- [1] HERDRICH, G. ; LÖHLE, S. ; AUWETER-KURTZ, M. ; ENDLICH, P. ; FERTIG, M. ; PIDAN, S. ; SCHREIBER, E.: IRS Ground-Testing Facilities: Thermal Protection System Development, Code Validation and Flight Experiment Development. In: *37th AIAA Thermophysics Conference*, 2004
- [2] POPE, Ronald B.: Stagnation–Point Convective Heat Transfer in Frozen Boundary Layers. In: *AIAA J.* 6 (1968), Nr. 4, S. 619–626
- [3] LAUX, Torsten: *Untersuchungen zur Hochtemperaturoxidation von Siliziumkarbid in Plasmaströmungen (Investigations of the High-temperature Oxidation of Silicon Carbide in Plasma Flows)*, University of Stuttgart, Doctoral thesis, 2004
- [4] HABIGER, Harald: *Elektrostatistische Sonden und Fabry-Perot-Interferometrie zur Untersuchung von lichtbogenbeheizten Plasmen für Triebwerksanwendungen und Wiedereintrittssimulation*. Institut für Raumfahrtsysteme, Universität Stuttgart, Dissertation, 1994
- [5] AUWETER-KURTZ, Monika ; WEGMANN, Thomas: Overview of IRS Plasma Wind Tunnel Facilities. In: *Measurement Techniques for High Enthalpy and Plasma Flows*. RTO/NATO, 2000